

This is the accepted manuscript made available via CHORUS. The article has been published as:

Protected Nodal Electron Pocket from Multiple-Q Ordering in Underdoped High Temperature Superconductors

N. Harrison and S. E. Sebastian

Phys. Rev. Lett. **106**, 226402 — Published 31 May 2011

DOI: [10.1103/PhysRevLett.106.226402](https://doi.org/10.1103/PhysRevLett.106.226402)

Protected nodal electron pocket from multiple- \mathbf{Q} ordering in underdoped high temperature superconductors

N. Harrison¹, S. E. Sebastian²

¹*National High Magnetic Field Laboratory, Los Alamos National Laboratory, MS E536, Los Alamos, New Mexico 87545*

²*Cavendish Laboratory, Cambridge University, JJ Thomson Avenue, Cambridge CB3 0HE, U.K*

(Dated: April 28, 2011)

A multiple wavevector (\mathbf{Q}) reconstruction of the Fermi surface is shown to yield a profoundly different electronic structure to that characteristic of single wavevector reconstruction, despite their proximity in energy. We consider the specific case in which ordering is generated by $\mathbf{Q}_x = [2\pi a, 0]$ and $\mathbf{Q}_y = [0, 2\pi b]$ (in which $a = b = \frac{1}{4}$) – similar to those identified in neutron diffraction and scanning tunneling microscopy experiments, and more generally show that an isolated pocket adjacent to the nodal point $\mathbf{k}_{\text{nodal}} = [\pm\frac{\pi}{2}, \pm\frac{\pi}{2}]$ is a protected feature of such a multiple- \mathbf{Q} model, potentially corresponding to the nodal ‘Fermi arcs’ observed in photoemission and the small size of the electronic heat capacity found in high magnetic fields – importantly, containing electron carriers which can yield negative Hall and Seebeck coefficients observed in high magnetic fields.

PACS numbers: PACS numbers: 71.18.+y, 75.30.fv, 74.72.-h, 75.40.Mg, 74.25.Jb

It has been challenging to identify the origin of small Fermi surface pockets observed by quantum oscillations in underdoped $\text{YBa}_2\text{Cu}_3\text{O}_{6+x}$ [1–4], given the absence of a unique expectation for the electronic structure from theoretical predictions in this regime [5]. While the details of the ordering differs between models, all translational symmetry-breaking models proposed thus far involve a single translational vector \mathbf{Q} [6] causing them to yield Fermi surface topologies with the same universal features – hole pockets and/or open sheets at the nodal point $\mathbf{k}_{\text{nodal}} = [\pm\frac{\pi}{2}, \pm\frac{\pi}{2}]$ in the extended Brillouin zone (BZ) and the possibility of an electron pocket at the antinodal point $\mathbf{k}_{\text{antinodal}} = [\pi, 0]$ & $[0, \pi]$. It becomes important to search for new models outside the realm of these universal features, which have difficulty simultaneously capturing the high field negative Hall and Seebeck coefficients [2] (interpreted in terms of an antinodal electron pocket [6]) and the pseudogap at the same location in zero field observed by ARPES and scanning tunneling spectroscopy (STM) [7–9]. While it has been suggested that translational symmetry breaking models may only be relevant in the high magnetic field regime of quantum oscillations, experiments have yet to establish the effect of a field in changing the electronic structure [10, 11].

Here we introduce a new possibility which we suggest is more applicable to the experimental situation in the underdoped cuprates. We show that multiple- \mathbf{Q} charge ordering yields a Fermi surface consisting of a protected electron pocket at the nodes – rather surprisingly, while the multiple- \mathbf{Q} charge ordering solution is argued to be close in energy to the single- \mathbf{Q} charge ordering solution [12], the consequences for electronic structure are profoundly different. In the case of underdoped $\text{YBa}_2\text{Cu}_3\text{O}_{6+x}$, a single electron pocket at the nodes produced by a range of coupling strengths in this model is most consistent with the single type of carrier pocket revealed by chemical potential quantum oscilla-

tions [13], and the density-of-states concentrated chiefly at the nodes in ARPES [7, 8] and in-field heat capacity experiments [11]; indeed the electron character of this pocket also yields negative Hall and Seebeck coefficients as experimentally observed [2]. We consider the case in which two orthogonal vectors $\mathbf{Q}_x = [2\pi a, 0]$ and $\mathbf{Q}_y = [0, 2\pi b]$ with $a \approx b \approx \frac{1}{4}$ lead to a ≈ 16 -fold reduction in the size of the BZ. Despite the aggregation of holes at $\mathbf{k}_{\text{nodal}}$ in the extended BZ, their density exceeds 50 % of the reconstructed BZ cross-section at the dopings relevant for quantum oscillation studies [1, 2] – the electron pocket resulting from a > 50 % filling of the folded band with holes. Unlike the antinodal electron pocket predicted by single- \mathbf{Q} models [6], the electron pocket found here incorporates the nodal ‘arc’ region of the Fermi surface (see Fig. 1) seen in ARPES [7, 8].

Evidence for ordering at wavevectors \mathbf{Q}_x and \mathbf{Q}_y is found in neutron diffraction [14] and STM [15, 16] measurements, with the possibilities including domains of unidirectional spin/charge stripes [17], stripes alternating on consecutive layers [18] or multiple- \mathbf{Q} charge ordering without a static spin component [7, 16, 19]. The latter may be relevant in underdoped $\text{YBa}_2\text{Cu}_3\text{O}_{6+x}$ where neutron scattering experiments find evidence for quasi-static spin ordering at oxygen compositions ($x < 0.45$, corresponding to hole dopings $\delta \lesssim 8$ %) lower than those in which quantum oscillations are observed [20], while charge ordering is observed at the same and higher dopings (orthogonal [21] and parallel [22] to the chain direction respectively). Furthermore, the observation of spin zeroes in magnetic quantum oscillation experiments is more easily explained by a scenario involving long range ordering of only the charge degrees of freedom [4].

We show in Fig. 1 how multiple- \mathbf{Q} charge ordering model and single- \mathbf{Q} charge ordering scenarios, while close in energy [12], lead to profoundly different electronic

structures. If one considers the single- \mathbf{Q} Hamiltonian

$$H_1 = \begin{pmatrix} \varepsilon & V & 0 & V \\ V & \varepsilon_{\mathbf{Q}_x} & V & 0 \\ 0 & V & \varepsilon_{2\mathbf{Q}_x} & V \\ V & 0 & V & \varepsilon_{3\mathbf{Q}_x} \end{pmatrix} \quad (1)$$

for example, in which V is the coupling and $\varepsilon_{\mathbf{Q}_x}$ represents the electronic dispersion $\varepsilon(\mathbf{k})$ [23, 24] translated by $\mathbf{Q}_x = [\frac{\pi}{2}, 0]$ [6], then susceptibility to gap formation (or approximate Fermi surface ‘nesting’) is realized only near $\mathbf{k} = [0, \pi \pm \frac{\pi}{4}]$ in the extended BZ: not $\mathbf{k} = [\pi \pm \frac{\pi}{4}, 0]$ (see Fig. 1a). Diagonalization of H_1 yields open Fermi surface sheets (see Fig. 1b). By contrast, on considering simultaneous translations by \mathbf{Q}_x and \mathbf{Q}_y , gap formation can occur both at $\mathbf{k} = [\pi \pm \frac{\pi}{4}, 0]$ and $[0, \pi \pm \frac{\pi}{4}]$ (see Fig. 1c). The open sheets of the single- \mathbf{Q} model give way to a small Fermi surface pocket in Fig. 1d (on introducing V), necessary to produce quantum oscillations [1, 2].

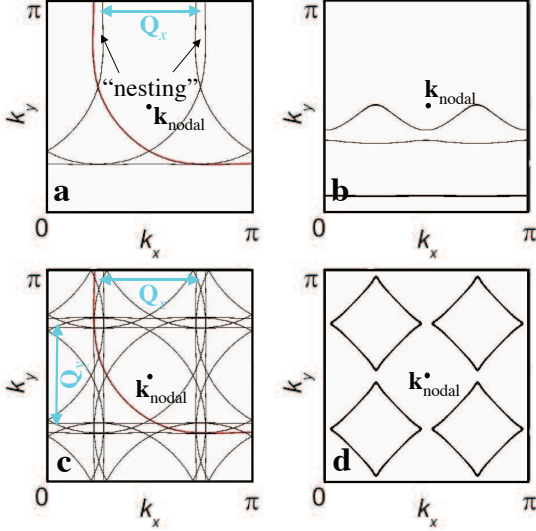


FIG. 1: **a** Quadrant of the unreconstructed Fermi surface (red) together with its translation by multiples of \mathbf{Q}_x (black) for $\delta = 8\%$. **b** Open sheets that result for $V/W = 0.1$. **c** Same quadrant of the unreconstructed BZ together with its translation by multiples of \mathbf{Q}_x and \mathbf{Q}_y . **d** Example showing how $V/W = 0.15$ leads to an electron pocket.

To construct a multiple- \mathbf{Q} ordering Hamiltonian, we consider all possible translations $\mathbf{k} \rightarrow \mathbf{k} + m\mathbf{Q}_x + n\mathbf{Q}_y$ in which m and n are integers to arrive at

$$H_2 = \begin{pmatrix} \varepsilon & V & V_{\text{II}} & V & V & V' & \dots \\ V & \varepsilon_{\mathbf{Q}_x} & V & V_{\text{II}} & V' & V & \dots \\ V_{\text{II}} & V & \varepsilon_{2\mathbf{Q}_x} & V & 0 & V' & \dots \\ V & V_{\text{II}} & V & \varepsilon_{3\mathbf{Q}_x} & V' & 0 & \dots \\ V & V' & 0 & V' & \varepsilon_{\mathbf{Q}_y} & V & \dots \\ V' & V & V' & 0 & V & \varepsilon_{\mathbf{Q}_y + \mathbf{Q}_x} & \dots \\ \vdots & \vdots & \vdots & \vdots & \vdots & \vdots & \ddots \end{pmatrix}. \quad (2)$$

We initially neglect higher order terms (i.e. $V' = V_{\text{II}} = 0$), consider V to be uniform and neglect a possible component of \mathbf{Q} orthogonal to the layers – similar Fermi surface results being envisaged [26] for multiple- \mathbf{Q} d-density-wave order [27] or charge stripes that alternate on consecutive layers [18]. We further consider the commensurate case where $a = b = \pm\frac{1}{4}$ (relevant to many STM and neutron diffraction experiments), which yields a 16×16 matrix and 16 bands upon diagonalization.

Despite $\mathbf{k}_{\text{nodal}} = [\pm\frac{\pi}{2}, \pm\frac{\pi}{2}]$ having 4 equivalent locations in the extended BZ, multiple- \mathbf{Q} ordering folds these onto a single point in the reconstructed BZ yielding a concentration only of holes. The small size of the reconstructed BZ causes this hole surface area (corresponding to a frequency in the range $900 < F_h = \frac{\hbar A_h}{2\pi e} < 1400$ T, where A_h is the k -space area) to exceed 50 % of the BZ area ($F_{\text{BZ}} = \frac{\hbar A_{\text{BZ}}}{2\pi e} \approx 1700$ T) for nominal hole dopings (in the range $8 \lesssim \delta \lesssim 11\%$) applicable to quantum oscillation experiments [1, 2] (see Fig. 1d). Band filling thus causes an electron pocket ($F_e = F_{\text{BZ}} - F_h$) to become a protected feature of multiple- \mathbf{Q} ordering.

Fermi surfaces calculated for different combinations of δ and ratios V/W of V to the electronic bandwidth W [23] are shown in Fig. 2. The complexity of the Fermi surface obtained at weaker couplings ($V/W < 0.15$) in Fig. 2 originates from the combined effects of imperfect ‘nesting’ and our neglect of the next nearest coupling V' between Fermi surfaces translated by $\mathbf{Q}_x \pm \mathbf{Q}_y$. These ‘nest’ almost as well (see Fig. 1c) as those with a relative translation of \mathbf{Q}_x or \mathbf{Q}_y . On including V' in Fig. 3a-c, a simple electron pocket is obtained for weaker coupling strengths. Finally, in Figs. 3d-f we include the effect of the ortho-II ordering potential V_{II} , which breaks the rotational symmetry of the Fermi surface. For the case considered ($V'/V = 0.6$ and $V/W = 0.05$), the electron pocket remains intact provided $V_{\text{II}}/V \leq 0.4$.

We compare features of the calculated Fermi surfaces in Fig. 2 (for $V/W \sim 0.15$) and Fig. 3 (for $V/W \sim 0.05$) with observed magnetic quantum oscillations in underdoped $\text{YBa}_2\text{Cu}_3\text{O}_{6+x}$ – a single carrier type of pocket unaccompanied by a significant reservoir being indicated by the observation of chemical potential quantum oscillations [13]. Both the frequency $F \approx 500$ T and effective mass $m^* \approx 1 - 2 m_e$ of the largest section obtained within the multiple- \mathbf{Q} model we propose are close to those in experiments [1–4] – no adjustment having been made to the tight-binding representation of the dispersion obtained from band structure calculations [23, 24]. As opposed to previously proposed single- \mathbf{Q} models in which two nodal hole pockets are contained in each bilayer BZ, the small size of the BZ in the multiple- \mathbf{Q} model we propose here causes it to contain only a single dominant electron pocket, yielding values for the Sommerfeld coefficient $\gamma_{\text{model}} \approx 5 - 9 \text{ mJmol}^{-1}\text{K}^{-2}$ (considering $V/W = 0.15$ and counting 2 bilayers) comparable to that $\gamma_{\text{exp}} \approx 5.3 \text{ mJmol}^{-1}\text{K}^{-2}$ obtained in heat capacity stud-

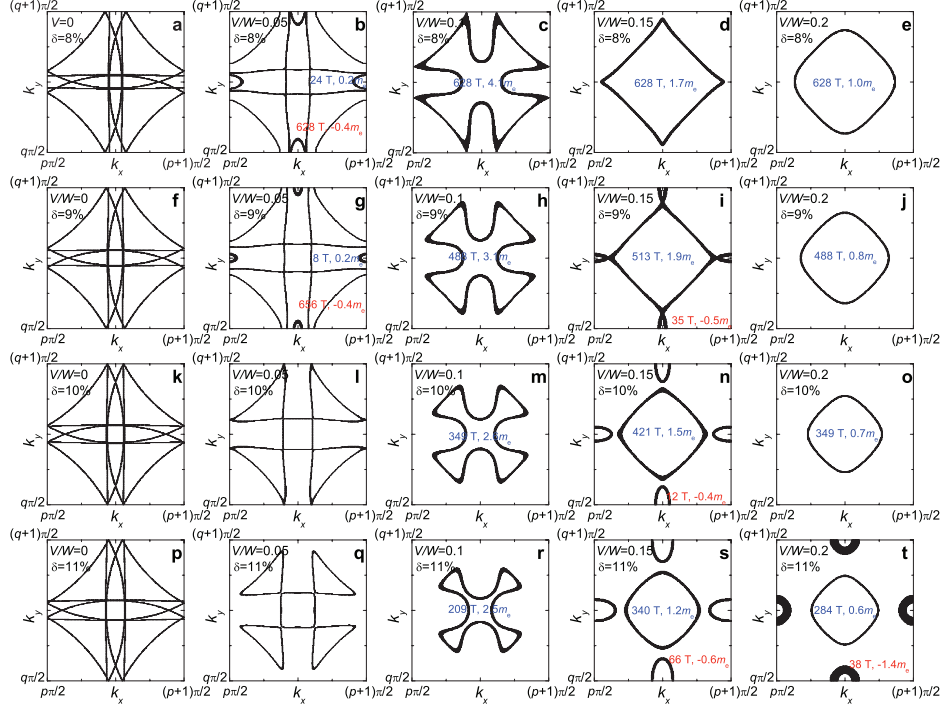


FIG. 2: Reconstructed Fermi surface according to Eqn (2) for $a = b = \pm \frac{1}{4}$, different ratios V/W and effective hole doping δ as indicated (assuming $V' = V_{II} = 0$). Also shown are the corresponding magnetic quantum oscillation frequencies according to Onsager's equation $F = A_k \hbar / 2\pi e$ (where A_k is the Fermi surface cross-section) and the corresponding band masses, where m_e is the free electron mass and a negative sign indicates holes. Line thicknesses are proportional to the inverse Fermi velocity.

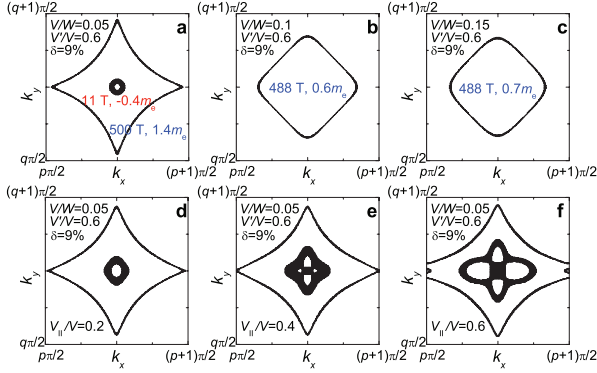


FIG. 3: **a, b** and **c**. Reconstructed Fermi surface according to Eqn (2) for $a = b = \pm \frac{1}{4}$ and different values of the ratio V/W as indicated for an effective hole doping $\delta = 9\%$ with $V'/V = 0.6$ and $V_{II} = 0$. **d, e** and **f**. Same as (**a**) but with the effect of different ortho-II potentials (V_{II}) included.

ies in strong magnetic fields [11]. The upper end of this range is caused by proximity to a Lifshitz transition at $\delta \approx 9\%$ when $V' = 0$ in the model. Furthermore, the electron-character of the largest predicted pocket over a broad range of dopings and couplings (being the only pocket for many combinations of V and δ) yields negative Hall and Seebeck coefficients, as seen in strong magnetic fields in underdoped $\text{YBa}_2\text{Cu}_3\text{O}_{6+x}$ [2]. The crossover to

positive Hall effect observed at elevated temperatures [2] could potentially be caused by loss of order [21].

Features of the multiple- \mathbf{Q} model are also compared with ARPES (and STM) Fermi surface measurements. Since the predicted electron pocket is constructed entirely from the nodal regions of $\varepsilon(\mathbf{k})$ and is also the largest pocket, the observation of Fermi arcs [7–9] would not be unexpected in this scenario. Specifically, as a consequence of coherence factors [28] and short correlation lengths [29], ARPES experiments may be expected to be sensitive chiefly to the portions of the reconstructed Fermi surface (black lines in Fig. 4) that overlap with the unreconstructed Fermi surface (depicted in grey).

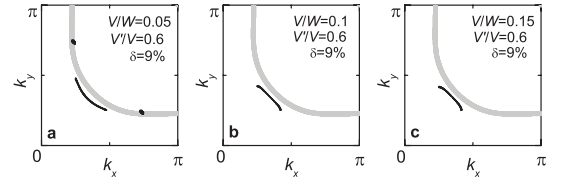


FIG. 4: The result of ‘unfolding’ the reconstructed Fermi surfaces in Figs. 3a-c so as to trace the origin of the Fermi surface segments to the original BZ (1/4 of which is shown).

In view of the Fermi surface comprising a single quasi-two dimensional pocket identified in recent quan-

tum oscillation experiments [13], the observed larger frequency [3] requires an additional explanation. The model we propose here offers some potential routes to explain the origin of such a larger frequency. Among these are magnetic breakdown frequencies resulting from tunneling across gaps in the Fermi surface — for instance a BZ frequency F_{BZ} [30]. A complete understanding of these effects, however, is complicated by the fact that the magnetization experiments are performed in the vortex state [3]. Magnetic breakdown (and the Hall effect) will also be sensitive to topological details, such as interlayer tunneling, bilayer coupling [31], V and the possible presence of small hole pockets at the BZ boundary.

In summary, we identify an electron pocket located at the nodal regions of the BZ as a universal feature of multiple- \mathbf{Q} charge ordering. A viable alternative is proposed to the previously proposed spin and/or charge models which lead to a combination of hole pockets at the nodes, electron pockets at the antinodes, and open sheets of Fermi surface. The applicability of this model to underdoped $\text{YBa}_2\text{Cu}_3\text{O}_{6+x}$ in which small Fermi surface pockets have been observed is particularly relevant given the recent discovery of charge order at high magnetic fields [21] — the size, location and carrier type of the Fermi surface topology expected within this model are shown to be better consistent with experimental observations than previously proposed single- \mathbf{Q} models. A further strength of the multiple- \mathbf{Q} model is that the electron pocket is formed from the lowest of the upper 8 bands in the multiple- \mathbf{Q} model (out of a total 16 bands), suggesting that this pocket will remain robust against the introduction of a strong Coulomb repulsion in the model.

We acknowledge DOE BES project “Science at 100 Tesla” and helpful advice from G. G. Lonzarich.

-
- [1] N. Doiron-Leyraud *et al.*, Nature **447**, 565 (2007); A. Audouard *et al.*, Phys. Rev. Lett. **103**, 157003 (2009); S. E. Sebastian *et al.*, Proc. Nat. Acad. Sci. USA **107**, 6175 (2010).
- [2] D. LeBoeuf *et al.*, Nature **450**, 533 (2007); D. LeBoeuf *et al.*, Phys. Rev. B **83**, 054506 (2011); F. Laliberté *et al.*, arXiv:1102.0984.
- [3] S. E. Sebastian *et al.*, Nature **454**, 200 (2008); S. E. Sebastian *et al.* Phys. Rev. B **81**, 214524 (2010).
- [4] B. J. Ramshaw *et al.*, N. Phys. **7**, 234 (2011); S. E. Sebastian, preprint arXiv:1103.4178 (2011).
- [5] M. R. Norman, Physics **3**, 86 (2010).
- [6] A. J. Millis and M. R. Norman, Phys. Rev. B **76**, 220503 (2007); S. Chakravarty, H. Y. Kee, Proc. Nat. Acad. Sci. USA **105**, 8835 (2008).
- [7] K. M. Shen *et al.* Science **307** 901(2005).
- [8] M. A. Hossain *et al.* Nature Phys. **4**, 527 (2008); A. Kanigel *et al.* Nature Phys. **2**, 447 (2006); H. Ding *et al.* Nature **382**, 51 (1996); A. Damascelli, Z. Hussain, Z. X. Shen, Rev. Mod. Phys. **75**, 473 (2003); T. Valla *et al.*, Science **314**, 1914 (2006); J. Chang *et al.*, N. J. Phys. **10**, 103016 (2008).
- [9] J. Lee *et al.*, Science **325**, 1099 (2009).
- [10] J. M. Tranquada *et al.* Phys. Rev. B **81**, 060506 (2010); A. D. LaForge *et al.*, Phys. Rev. B **81**, 064510 (2010).
- [11] S. C. Riggs *et al.*, Nature Phys. **7** 332 (2011).
- [12] A. Melikyan and M. R. Norman, arXiv: 1102.5443
- [13] S. E. Sebastian *et al.*, preprint arXiv:1103.4180 (2011).
- [14] J. M. Tranquada *et al.*, Nature **375**, 561(1995); M. Fujita *et al.*, Phys. Rev. Lett. **88**, 167008 (2002); J. M. Tranquada *et al.*, Phys. Rev. B **54**, 7489 (1996).
- [15] J. E. Hoffman *et al.* Science **295**, 466 (2002); T. Hanaguri *et al.*, Nature **430**, 1001 (2004).
- [16] K. McElroy *et al.*, Phys. Rev. Lett. **94**, 197005 (2005); W. D. Wise *et al.*, Nature Phys. **4**, 696 (2008).
- [17] J. A. Robertson *et al.* Phys. Rev. B **74**, 134507 (2006).
- [18] M. V. Zimmermann *et al.* Europhys. Lett **41**, 629 (1998); R. S. Markiewicz, Phys. Rev. B **71**, 220504 (2005); N. B. Christensen *et al.*, Phys. Rev. Lett. **98**, 197003 (2007).
- [19] Multiple-**Q** spin ordering with $\mathbf{Q}_s = [\pi(1 \pm \frac{1}{4}), \pi]$ & $[\pi, \pi(1 \pm \frac{1}{4})]$ is expected to yield a charge Bragg peak at $\mathbf{Q} = [\pm\pi/4, \pm\pi/4]$. Its absence could support either unidirectional spin stripe domains [17] or multiple-**Q** charge ordering without concomitant spin order.
- [20] D. Haug *et al.* New J. Phys. **12**, 105006 (2010).
- [21] M.-H. Julien, (Aspen Winter Conference, 2011).
- [22] X. Liu *et al.*, Phys. Rev. B **78**, 134526 (2008).
- [23] We use $\varepsilon = \varepsilon_0 + 2t_{10}[\cos ak_x + \cos bk_y] + 2t_{11}[\cos(ak_x + bk_y) + \cos(ak_x - bk_y)] + 2t_{20}[\cos 2ak_x + \cos 2bk_y]$ [24], with band width $W = 8t_{10} = 3$ eV and next nearest neighbor hoppings $t_{11}/t_{10} = -0.32$ and $t_{20}/t_{10} = 0.16$. The chemical potential is adjusted for each calculation to ensure compatibility with Luttinger's theorem.
- [24] O. K. Andersen *et al.*, Phys. Chem. Solids **56**, 1573 (1995).
- [25] M. Hashimoto *et al.* Nature Phys. **6**, 414 (2010).
- [26] The nodal 'arc' section of the Fermi surface is only weakly affected by the vanishing of V at the nodes [27], while stripes alternating on consecutive layers [18] introduce an additional periodicity in the interlayer direction – minimally impacting the in-plane topology.
- [27] K. Seo, H.-D. Chen, J. Hu, Phys. Rev. B **76**, 020511 (2007).
- [28] J.-X. Li, C.-Q. Wu, D.-H. Lee, Phys. Rev. B **74**, 184515 (2006).
- [29] N. Harrison, R. D. McDonald, J. Singleton, Phys. Rev. Lett. **99**, 206406 (2007).
- [30] Mg provides an example of a simple metal exhibiting magnetic breakdown and a BZ frequency in the magnetic susceptibility; J. W. Eddy Jr., R. W. Stark, Phys. Rev. Lett. **48**, 275 (1982).
- [31] Coupling between and within bonding and antibonding bands will yield a doubly degenerate frequency F_e and split frequencies $F_e \pm \Delta F$, respectively, where ΔF reflects the magnitude of the bilayer splitting in the nodal region.